

Some Simple Vacuum Polarization Phenomenology: $e^+e^- \rightarrow$ Hadrons;

The μ -Mesic Atom X-ray Discrepancy and $g_\mu - 2$

Stephen L. Adler
National Accelerator Laboratory
Batavia, Illinois 60510

and

The Institute for Advanced Study
Princeton, New Jersey 08540

ABSTRACT

We give a simple phenomenological analysis of hadronic and electronic vacuum polarization effects. We argue that the derivative of the hadronic vacuum polarization, evaluated in the space-like region, provides a useful meeting ground for comparing $e^+e^- \rightarrow$ hadron annihilation data (assumed to arise from one-photon annihilation) with the predictions of parton models and of asymptotically free field theories. Using dispersion relations to connect the annihilation and space-like regions, we discuss the implications in the space-like region of a constant e^+e^- annihilation cross section. In particular, we show that a flat cross section between $t = 25$ and $t = 81$ $(\text{GeV}/c)^2$ would provide strong evidence against a precociously asymptotic color triplet model for hadrons. We then turn to a consideration of the apparent discrepancy between observed and calculated

muonic atom X-ray transition energies. Specifically, we analyze the hypothesis of attributing this discrepancy to a deviation of the asymptotic electronic vacuum polarization from its expected value, a possibility which is compatible with all current high-precision tests of quantum electrodynamics. Under the additional technical assumption that the postulated discrepancy in the electronic vacuum polarization spectral function increases monotonically with t , the hypothesis predicts a decrease in the expected value of the muon magnetic moment anomaly $a_\mu = \frac{1}{2}(g_\mu - 2)$ of at least $-0.96 \cdot 10^{-7}$, which should be detectable in the next round of $g_\mu - 2$ experiments and which is substantially larger than likely uncertainties in the hadronic contribution to a_μ . By contrast, postulating a weakly coupled scalar boson ϕ to explain the muonic atom discrepancy would imply a (very small) increase in the expected value of a_μ . Both the vacuum polarization and scalar boson hypotheses (for $M_\phi \geq 1 \text{ MeV}$) predict a reduction of order 0.027 eV in the $2p_{\frac{1}{2}} - 2s_{\frac{1}{2}}$ transition energy in $[^4\text{He}, \mu]^+$, an effect which may be observable.

I. Introduction

A number of recent experiments have brought aspects of vacuum polarization phenomena to the fore. Most prominent are the measurements by the CEA and SLAC-LBL groups of an unexpectedly large cross section for $e^+e^- \rightarrow \text{hadrons}$,¹ which gives the absorptive part of the hadronic vacuum polarization. In another area of physics, measurements of muonic atom X-ray transition energies, undertaken to probe the asymptotic form of the

electronic vacuum polarization, appear to show a persistent deviation from theoretical expectations.² Forthcoming high-precision measurements of the muon magnetic moment anomaly $g_\mu - 2$ will provide an even more sensitive probe of the asymptotic electronic vacuum polarization, and of the hadronic vacuum polarization as well. We present in this paper simple phenomenological arguments which bear on the interpretation of both the annihilation and the muonic experiments. Although fundamentally different physical issues are at stake in the two classes of experiments, common elements of formalism make it natural to consider them together. In Section 2 we use dispersion relations to determine what the time-like region e^+e^- annihilation data say about the possibility of precocious asymptotic scaling in the space-like region of the hadronic vacuum polarization (assuming that the observed data do indeed result from one-photon annihilation). In Section 3 we analyze the muonic experiments, with the aim of distinguishing between the possibilities that the muonic atom X-ray discrepancies may arise from a discrepancy in the asymptotic electronic vacuum polarization, or from the existence of a weakly coupled light scalar boson. Some technical details are given in the Appendices.

2. Electron Positron Annihilation and Precocious Space-like Scaling.

The experimental data for electron positron annihilation into hadrons are conveniently expressed in terms of the ratio $R(t)$, defined as

$$R(t) = \frac{\sigma(e^+e^- \rightarrow \text{hadrons}; t)}{\sigma(e^+e^- \rightarrow \mu^+\mu^-; t)}, \quad (1)$$

with

$$\begin{aligned} \sigma(e^+e^- \rightarrow \mu^+\mu^-; t) &= \left(1 + \frac{2m_\mu^2}{t}\right) \left(1 - \frac{4m_\mu^2}{t}\right)^{\frac{1}{2}} \frac{4\pi\alpha^2}{3t} \\ &\approx \frac{4\pi\alpha^2}{3t} = \frac{87 \cdot 10^{-33} \text{ cm}^2}{t [\text{in } (\text{GeV}/c)^2]} \end{aligned} \quad (2)$$

and with t the virtual photon four-momentum squared. In Fig. 1 we have plotted (versus $E = t^{\frac{1}{2}}$) a smooth interpolation through all available experimental data for R in the continuum region (excluding the ρ , ω and ϕ vector meson contributions). The CEA and SLAC-LBL data points are indicated,¹ while the portion of the curve below $t = 2.5$ is taken from the "eyeball" fit given by Silvestrini.³ When replotted versus t , the data for $R(t)$ rise approximately linearly, indicating a roughly constant hadronic annihilation cross section of $21 \cdot 10^{-33} \text{ cm}^2$. Assuming that single photon annihilation is indeed being measured, this behavior strongly contradicts the asymptotic behavior expected on the basis of parton or of asymptotically free field theory models of the hadrons, which predict

$$R \sim C, \quad t \rightarrow \infty \quad (3)$$

with the constants C tabulated in Table I. However, it can always be argued that while precocious asymptotic behavior is expected from the SLAC scaling results in the space-like region, the annihilation reaction involves the time-like region, in which asymptotic predictions may be approached much more slowly. This objection naturally raises the question of determining what the annihilation data tell us about behavior in the space-like region.

To answer this question we consider the renormalized hadronic vacuum polarization tensor ($t = q^2$)

$$\Pi_{\mu\nu}^{(H)}(q) = (q_\mu q_\nu - t g_{\mu\nu}) \Pi^{(H)}(t), \quad (4)$$

which obeys the dispersion relation

$$\Pi^{(H)}(t) = t \int_{4m_\pi^2}^{\infty} \frac{du}{u} \frac{\frac{1}{\pi} \text{Im} \Pi^{(H)}(u)}{u-t}, \quad (5)$$

and which is related to the electron-positron annihilation cross section into hadrons by

$$\sigma(e^+ e^- \rightarrow \text{hadrons}; u) = \frac{1}{u} \text{Im} \Pi^{(H)}(u) \times (\text{known constants}). \quad (6)$$

Rather than using Eq. (5) directly, we consider its first derivative

$$\frac{d}{dt} \Pi^{(H)}(t) = \int_{4m_\pi^2}^{\infty} du \frac{\frac{1}{\pi} \text{Im} \Pi^{(H)}(u)}{(u-t)^2}, \quad (7)$$

which on substituting Eq. (6) and using Eqs. (1) and (2) can be rewritten as

$$\frac{d}{dt} \Pi^{(H)}(t) = \int_{4m_\pi^2}^{\infty} du \frac{R(u)}{(u-t)^2} \times (\text{known constants}). \quad (8)$$

Restricting ourselves to the space-like region $t = -s$, $s > 0$ and rescaling to remove the constant factors, we obtain from Eq. (8) our basic relation

$$\Gamma(-s) \equiv \int_{4m_\pi^2}^{\infty} \frac{du R(u)}{(s+u)^2} = \frac{d}{dt} \Pi^{(H)}(t) \Big|_{t=-s} \times (\text{known constants}). \quad (9)$$

The quantity $T(-s)$ has two desirable properties which make it suitable for studying the implications of the annihilation reaction for space-like-region behavior:

- (i) The integrand in Eq. (9) is positive definite, and so omitting the high energy tail of the integral makes an error of known sign. Specifically, if experimental data on R are available only up to a maximum momentum transfer squared t_C , and if we define

$T_{\text{obs}}(-s)$ by

$$T_{\text{obs}}(-s) = \int_{\frac{2}{\pi}}^{t_C} \frac{du R(u)}{(s+u)^2}, \quad (10)$$

then we have

$$T_{\text{obs}}(-s) \leq T(-s), \quad 0 \leq s < \infty. \quad (11)$$

- (ii) It is the quantity $T(-s)$ for which parton models and asymptotically free field theories most directly make predictions;⁴ the asymptotic predictions for R are always obtained from the prediction for $T(-s)$ by a dispersion relation argument, which is bypassed if we use $T(-s)$ as the primary phenomenological object. In a model in which R asymptotically approaches C , we have

$$T_{\text{th}}(-s) \sim \frac{C}{s}, \quad s \rightarrow \infty. \quad (12)$$

In asymptotically free field theories, the leading logarithmic correction to Eq. (12) is also determined. Specifically, in the $SU(3) \otimes SU(3)$ ¹ color triplet model of the hadrons, one has⁴

$$\Gamma_{\text{th}}(-s) \sim \frac{2}{s} \left[1 + \frac{4}{9} \frac{1}{\ln(s/s_0)} + \dots \right], \quad (13)$$

with s_0 an arbitrary momentum scale which, in the numerical work, we will take as 2 (GeV/c)^2 .

Before proceeding to numerical applications, let us briefly discuss the question of subtractions. Clearly, if the one photon annihilation cross section were to remain constant as $t \rightarrow \infty$, we would have $R(u) \propto u$, $u \rightarrow \infty$ and the integral in Eq. (9) would need an additional subtraction to be well-defined.⁵ However, such behavior of R would in itself contradict Eq. (3) for all values of C , and hence would rule out all versions of the parton model or of asymptotically free field theories. On the other hand, if Eq. (3) is true for any finite C then the integral in Eq. (9) converges as it stands, and provides a suitable medium for comparing the annihilation data with theoretical expectations in the space-like region. Note that a constant subtraction term in Eq. (5), which would be present if we renormalize at a point other than $t = 0$, would not contribute to the t -derivative in Eq. (7); hence the renormalization prescription is not a possible source of ambiguity.

We turn now to the numerical results. In Fig. 2 we plot $\Gamma_{\text{obs}}(-s)$ [in units where unity = $(1 \text{ GeV/c})^2$], as obtained from all experimental data up to $t_C = 25 \text{ (GeV/c)}^2$ according to the formula⁶

$$T_{\text{obs}}(-s) = T^{\omega+\phi}(-s) + T^{\rho}(-s) + T^{\text{cont}(1)}(-s),$$

$$T^{\omega+\phi}(-s) = \frac{9\pi}{\alpha^2} \sum_{V=\omega, \phi} \frac{M_V \Gamma(V \rightarrow e^+ e^-)}{(s + M_V^2)^2}, \quad (14)$$

$$T^{\rho}(-s) = \int_{4m_{\pi}^2}^{\infty} \frac{dt}{(s+t)^2} \frac{1}{4} \left(1 - \frac{4m_{\pi}^2}{t}\right)^{3/2} |F_{\pi}(t)|^2,$$

$$T^{\text{cont}(1)}(-s) = \int_{0.39}^{25} \frac{dt}{(s+t)^2} R(t).$$

The vector meson parameters appearing in Eq. (14) are given in Appendix A, while $R(t)$ is the continuum contribution to R graphed in Fig. 1. In Fig. 3 we plot a family of curves, obtained by assuming that for $25 \leq t \leq t_C$ the annihilation cross section $\sigma(e^+ e^- \rightarrow \text{hadrons}; t)$ remains constant at $21 \cdot 10^{-33} \text{ cm}^2$. That is, we take

$$T_{\text{obs}}(-s) = T^{\omega+\phi}(-s) + T^{\rho}(-s) + T^{\text{cont}(1)}(-s) + T^{\text{cont}(2)}(-s),$$

$$\begin{aligned} T^{\text{cont}(2)}(-s) &= \int_{25}^{t_C} \frac{dt}{(s+t)^2} 5.94 \left(\frac{t}{25}\right) \\ &= 0.24 \left[\ln \left(\frac{s+t_C}{s+25} \right) - s \frac{(t_C-25)}{(s+t_C)(s+25)} \right]. \end{aligned} \quad (15)$$

Rather than plotting $T_{\text{obs}}(-s)$ we have plotted the comparison ratio $T_{\text{obs}}(-s) / T_{\text{th}}(-s)$, with $T_{\text{th}}(-s)$ the color triplet prediction of Eq. (13). The $t_C = 25$ curve is just the curve of Fig. 2 divided by Eq. (13); since this curve lies below 1 the existing annihilation data do not yet challenge the color triplet model in the space-like region. [However, since the

$t_C = 25$ curve lies well above $1/3$, the existing data already definitively rule out a precociously asymptotic simple quark triplet model.] Evidently, the curves in Fig. 3 rise rapidly with t_C , and show that if the annihilation cross section should remain constant at roughly $21 \cdot 10^{-33} \text{ cm}^2$ in the region $25 \leq t \leq 81$ which will be accessible at SPEAR II, a precociously asymptotic color triplet model would be ruled out in the space-like region.

To explore the consequences of an annihilation cross section which remains flat up to large t_C , we ignore the vector meson contributions to T_{obs} and approximate $T^{\text{cont}(1)}(-s)$ by taking $R(t) \approx 0$, $t < 2$; $R(t) \approx 0.24t$, $2 \leq t \leq 25$, giving the simple analytic expression

$$\begin{aligned}
 T_{\text{obs}}(-s) &= \int_2^{t_C} \frac{dt}{(s+t)^2} 0.24t \\
 &= 0.24 \left[\ln \left(\frac{s+t_C}{s+2} \right) - s \frac{(t_C-2)}{(s+t_C)(s+2)} \right] \\
 &\approx 0.24 \left[\ln \left(\frac{s+t_C}{s} \right) - \frac{t_C}{s+t_C} \right].
 \end{aligned} \tag{16}$$

Hence,

$$\begin{aligned}
 \frac{T_{\text{obs}}(-s)}{\frac{1}{s}} &\approx R(t_C) f(z), \\
 R(t_C) &= 0.24 t_C,
 \end{aligned} \tag{17}$$

$$f(z) = \frac{1}{2} \ln(1+z) - \frac{1}{1+z}, \quad z = t_C/s.$$

A simple maximization shows that $f(z)$ attains a maximum of 0.22 at

$z_M^{-1} = s_M/t_C = 0.46$, and falls to half maximum at $z_L^{-1} = s_L/t_C = 0.053$ and $z_U^{-1} = s_U/t_C = 3.22$. That is, $T_{\text{obs}}(-s)/s^{-1}$ reaches a maximum value

$$[T_{\text{obs}}(-s)/s^{-1}]^{\text{MAX}} = 0.22 \times 0.24 t_C = 0.053 t_C \quad (18a)$$

and lies above half this value in the wide range

$$0.053 t_C \leq s \leq 3.22 t_C . \quad (18b)$$

To give a concrete illustration, if $\sigma(e^+e^- \rightarrow \text{hadrons}; t)$ should remain constant up to the maximum t_C of 900 obtainable in a 15 GeV/c on 15 GeV/c storage ring, the maximum of $T_{\text{obs}}(-s)/s^{-1}$ would be $0.053 \times 900 = 48!$ This would exclude by a factor of two parton or asymptotically free models with $C \leq 24$, thus covering just about every model which has been seriously proposed.

3. The μ -Mesic Atom X-ray Discrepancy and $g_\mu - 2$.

Recent studies of the transition energies between large circular orbits in μ -mesic atoms have shown persistent discrepancies between theory and experiment. Because the muonic orbits in question lie well outside the nucleus and well inside the innermost K-shell electrons, one believes that nuclear size and electron screening corrections can be reliably estimated. In particular, the disputed nuclear size corrections to the vacuum polarization potential have been reevaluated recently by three independent groups,⁷ in good agreement with one another. A survey of all known theoretical corrections has been given by Watson and Sundarasan² (see also Rafelski, et al.⁸), with the conclusion

that all important effects within the standard electrodynamic theory have been correctly taken into account. On the experimental side, independent measurements by the groups of Dixit, Anderson, et al.⁹ and of Walter, Vuilleumier, et al.¹⁰ agree on X-ray transition energies which deviate by two standard deviations from the theoretical predictions, as summarized in Table II. While it may still turn out that systematic experimental errors or errors or omissions in the theoretical calculations account for the discrepancy, we will assume this not to be the case. Rather, we will treat the discrepancy as a real effect, to be explained by modifications in the conventional theory.

The unique aspect of the muonic atom transition energies is that, because the muonic orbits lie well inside the electron Compton wavelength, they receive a large contribution from the electronic vacuum polarization potential and (unlike the more accurate Lamb shift experiments) they probe the asymptotic structure of this potential. Motivated by this observation, our principal focus will be to explore the possibility that the observed X-ray energy discrepancy arises from a nonperturbative deviation of the electronic vacuum polarization from its expected value. Such an effect is qualitatively expected (but with unknown quantitative form) if recent speculations that the fine structure constant α is electrodynamically determined prove to be correct.¹¹ We will also briefly consider an alternative explanation which has been advanced to explain the X-ray discrepancy, the possible existence of a weakly coupled light scalar boson.¹²

To calculate the effects of a possible discrepancy in the electronic vacuum polarization we start from the Uehling potential written in spectral form,

$$V(r) = -Z \frac{\alpha^2}{3\pi} \int_{\frac{2}{4m_e}}^{\infty} \frac{dt}{t} \left(\frac{e^{-t^{\frac{1}{2}}r}}{r} \right) \rho_e[t] , \quad (19)$$

$$\rho_e[t] = \left(1 + \frac{2m_e^2}{t} \right) \left(1 - \frac{4m_e^2}{t} \right)^{\frac{1}{2}} .$$

If we now assume that the spectral function $\rho_e[t]$ is changed by nonperturbative effects¹³ to $\rho_e[t] + \delta\rho[t]$, then V is replaced by $V + \delta V$, with

$$\delta V(r) = -Z \frac{\alpha^2}{3\pi} \int_{\frac{2}{4m_e}}^{\infty} \frac{dt}{t} \left(\frac{e^{-t^{\frac{1}{2}}r}}{r} \right) \delta\rho[t] . \quad (20)$$

This potential contributes to μ -mesic atom energies through the diagram shown in Fig. 4(a). Since Eq. (20) is a small perturbation and since the muon orbits of interest are appreciably larger in radius than the muon Compton wavelength, in evaluating matrix elements of $\delta V(r)$ we make the approximation of using non-relativistic hydrogenic muon wave functions. [The same approximation applied to Eq. (19) yields the Uehling energy shifts for all of the levels in Table II to an accuracy of about 5%.]¹⁴ Thus we take

$$R_{n, n-1}(r) = \left\{ \left(\frac{2Z}{na_0} \right)^3 \frac{1}{(2n)!} \right\}^{\frac{1}{2}} e^{-\frac{Z}{na_0}r} \left(\frac{2Zr}{na_0} \right)^{n-1} , \quad (21)$$

$$a_0 = \frac{1}{\alpha m_\mu} ,$$

giving for the change in transition energy produced by $\delta V(r)$,

$$\delta E_Y = \delta E_n - \delta E_{n-1} = \int_0^\infty r^2 dr [R_{n n-1}(r)^2 - R_{n-1 n-2}(r)^2] \delta V(r). \quad (22)$$

Substituting Eq. (20) into Eq. (22), evaluating the r-integral, and using $\alpha^2/(3\pi a_0) = 4.35 \text{ eV}$, we find

$$\overline{\delta E}_Y \equiv \frac{\delta E_Y}{4.35 \text{ eV} Z^2 \left[\frac{1}{(n-1)^2} - \frac{1}{n^2} \right]} = \int_0^\infty \frac{dt}{4m_e^2} f_Y[t] \delta\rho[t], \quad (23)$$

$$f_Y[t] = \left[\frac{1}{(n-1)^2} - \frac{1}{n^2} \right]^{-1} \left\{ \frac{1}{(n-1)^2} \left[1 + \left(\frac{t}{4m_\mu^2} \right)^{\frac{1}{2}} \frac{n-1}{Z\alpha} \right]^{-2(n-1)} - \frac{1}{n^2} \left[1 + \left(\frac{t}{4m_\mu^2} \right)^{\frac{1}{2}} \frac{n}{Z\alpha} \right]^{-2n} \right\},$$

$$f_Y[0] = 1.$$

Finally, for convenience in doing the numerical work we make the change of variable

$$t = 4m_e^2 e^w, \quad (24)$$

giving the formulas

$$\overline{\delta E}_Y = \int_0^\infty dw f_Y(w) \delta\rho(w), \quad (25)$$

$$f_Y(w) = f_Y[4m_e^2 e^w], \quad \delta\rho(w) = \delta\rho[4m_e^2 e^w].$$

Evidently, in the non-relativistic approximation which we are using, the shifts in the transition energy δE_Y are j-independent, and hence the two transitions for each n,l measure the same weighted integral

of $\delta\rho(w)$. Thus, for purposes of comparison with Eq. (25) we average the two discrepancy values for each n, ℓ , as shown in the fourth column of Table II.¹⁵ The "reduced discrepancies" $\delta\bar{E}_\gamma$ introduced in Eq. (23) are tabulated in the final column of Table II.

Before proceeding further with our discussion of the μ -mesic X-ray discrepancy, let us turn to consider another electrodynamic measurement which is sensitive to the asymptotic electronic vacuum polarization, the muon $g_\mu - 2$ experiment. Here the conjectured deviation in the electronic vacuum polarization spectral function contributes through the diagram of Fig. 4(b). Introducing the standard definition

$$a_\mu = \frac{1}{2}(g_\mu - 2) \quad (26)$$

and using well-known formulas¹⁶ for the photon spectral-function contribution to a , we find that changing the electron vacuum polarization spectral function induces a $g_\mu - 2$ discrepancy

$$\delta a_\mu = \frac{\alpha^2}{3\pi^2} \int_{\frac{2}{4m_e}}^{\infty} \frac{dt}{t} \frac{1}{2} f_a[t] \delta\rho[t], \quad (27)$$

$$f_a[t] = 2 \int_0^1 dx \frac{x^2(1-x)}{x^2 + (1-x)t/m_\mu^2}, \quad f_a[0] = 1.$$

Using $\alpha^2/(3\pi^2) = 1.80 \cdot 10^{-6}$ and making the change of variable of Eq. (24), we get the convenient formula

$$\delta a_{\mu} = 1.80 \cdot 10^{-6} \frac{1}{2} \int_0^{\infty} dw f_a(w) \delta \rho(w) , \quad (28)$$

$$f_a(w) = f_a [4 m_e^2 e^w] .$$

The result of carrying out the integrations in the expression for $f_a(t)$ is given in Appendix B.

Let us now return to our analysis of the μ -mesic X-ray discrepancy. The kernels $f_{\gamma}(w)$ for four representative transitions are plotted in Fig. 5. Our numerical evaluation shows that the six transitions listed in Table III have weight functions f_{γ} which are nearly identical (their spread around curve b in Fig. 5 is less than one third of the spacing between curve b and curve a); averaging the weight functions for these transitions gives the function \bar{f}_{γ} plotted in Fig. 6. Substituting the average of the reduced discrepancies for these six transitions into Eq. (25), we find

$$\begin{aligned} (54.5 \pm 10) \cdot 10^{-3} &= \text{Average of six } (-\delta \bar{E}_{\gamma}) \\ &= - \int_0^{\infty} dw \bar{f}_{\gamma}(w) \delta \rho(w) , \end{aligned} \quad (29)$$

indicating that the sign of the discrepancy corresponds to a reduction in the electronic vacuum polarization spectral function from its usual value of Eq. (19). Referring back to Fig. 6, we note that the function f_a is always greater than \bar{f}_{γ} . Hence if we assume that $\delta \rho(w)$ is always of negative sign in the region where f_a and \bar{f}_{γ} are non-zero [as might reasonably be expected if we are just entering a new region of physics where the discrepancy $\delta \rho(w)$ is turning on] we learn that

$$\int_0^{\infty} dw f_a(w) \delta\rho(w) \leq -(54.5 \pm 10) \cdot 10^{-3} . \quad (30)$$

Comparing Eq. (30) with Eq. (28) we then get an inequality for the $g_{\mu} - 2$ discrepancy,

$$\delta\rho \leq 0 \rightarrow \begin{cases} \delta a_{\mu} \leq -1.80 \cdot 10^{-6} \frac{1}{2} (54.5 \pm 10) \cdot 10^{-3} = -(0.49 \pm 0.09) \cdot 10^{-7}, \\ \frac{\delta a_{\mu}}{a_{\mu}} \leq -42 \pm 8 \text{ ppm}. \end{cases} \quad (31)$$

A stronger prediction follows if, in addition to our assumption on the sign of $\delta\rho$, we assume that the magnitude of $\delta\rho$ increases monotonically with t [again as might reasonably be expected for an effect just turning on]. Then defining

$$\bar{f}_{\gamma}(w) = 0, \quad w < 0, \quad (32)$$

we find that we can represent $f_a(w)$ as a superposition of displaced curves \bar{f}_{γ} ,

$$f_a(w) = 1.016 \bar{f}_{\gamma}(w) + \int_0^{10.2} dw' c(w') \bar{f}_{\gamma}(w-w'), \quad (33)$$

with the positive weight function c plotted in Fig. 6. Multiplying by $\delta\rho(w)$ and integrating we get

$$\begin{aligned} \int_0^{\infty} dw f_a(w) \delta\rho(w) &= 1.016 \int_0^{\infty} dw \bar{f}_{\gamma}(w) \delta\rho(w) \\ &+ \int_0^{10.2} dw' c(w') \int_0^{\infty} dw \bar{f}_{\gamma}(w-w') \delta\rho(w) . \end{aligned} \quad (34)$$

But using Eq. (32) and the assumed monotonicity of $\delta\rho$, we get

$$\int_0^{\infty} dw \bar{f}_Y(w-w') \delta\rho(w) = \int_0^{\infty} dw \bar{f}_Y(w) \delta\rho(w+w') \leq \int_0^{\infty} dw \bar{f}_Y(w) \delta\rho(w) \quad , \quad (35)$$

and so we learn

$$\int_0^{\infty} dw f_a(w) \delta\rho(w) \leq [1.016 + \int_0^{10.2} dw' c(w')] \int_0^{\infty} dw \bar{f}_Y(w) \delta\rho(w) = 2.00 \int_0^{\infty} dw \bar{f}_Y(w) \delta\rho(w) \quad . \quad (36)$$

Thus adding the assumption of monotonicity doubles the prediction of Eq. (30),

giving

$$\left. \begin{array}{l} \delta\rho \leq 0 \\ |\delta\rho| \uparrow \end{array} \right\} \Rightarrow \left. \begin{array}{l} \delta a_{\mu} \leq -(0.98 \pm 0.18) \cdot 10^{-7} \\ \frac{\delta a_{\mu}}{a_{\mu}} \leq -84 \pm 16 \text{ ppm} \end{array} \right. \quad . \quad (37)$$

Eq. (37) is the principal result of our analysis.

Two remarks about Eq. (37) are in order. First, the discrepancy in a_{μ} predicted in Eq. (37) is compatible, within errors, with the present agreement of experiment with the conventional electrodynamic prediction for a_{μ} ,¹⁷

$$a_{\mu}(\text{expt}) - a_{\mu}(\text{conventional QED}) = (2.5 \pm 3.1) \cdot 10^{-7} \quad . \quad (37)$$

However, it should be readily observable in the next $g_{\mu} - 2$ experiment, where it is anticipated¹⁷ that the current experimental error of $\pm 3.1 \cdot 10^{-7}$

(= ± 270 ppm in $\delta a_\mu / a_\mu$) will be reduced by a factor of 20. Second, the predicted effect is substantially larger than the likely remaining uncertain contributions to a_μ . Specifically, these are:

- (i) The 8th order electrodynamic contribution to a_μ , which has been variously estimated¹⁸ as $6 - 7 \cdot 10^{-9}$, with an uncertainty of perhaps a few parts in 10^{-9} .
- (ii) The uncertainty in the hadronic contribution to a_μ . Including the ρ , ω and ϕ resonances and integrating the e^+e^- annihilation continuum up to $t_C = 25$ gives a known hadronic contribution of $71 \cdot 10^{-9}$ with an estimated uncertainty of $\pm 7 \cdot 10^{-9}$ (See Appendix B). The unknown contribution of the e^+e^- annihilation continuum beyond $t_C = 25$ will of course depend on the behavior of $R(t)$ in that region. To get a crude estimate, let us make the (hopefully extreme) assumption that $R(t)$ rises linearly up to $t = (460)^2$, where the one photon annihilation cross section violates the $J=1$ unitarity limit,¹⁹ and cut off the integral at this point. This procedure suggests a bound on the high-energy hadronic contribution to a_μ of $15 \cdot 10^{-9}$. (Again see Appendix B).
- (iii) Unified gauge theories of the weak and electromagnetic interactions which do not have charged heavy leptons typically give contributions²⁰ to a_μ in the range from a few to ten parts in 10^{-9} . Specifically, the Weinberg-Salam $SU(2) \otimes U(1)$ model predicts a contribution to a_μ of less than $9 \cdot 10^{-9}$. Thus, from (i), (ii) and (iii) we conclude that the sum of unknown contributions to a_μ is likely to be no bigger than $\sim 35 \cdot 10^{-9}$, and hence should not mask the effect predicted in Eq. (37).

Although we have shown that the inequality of Eq. (37) does not contradict the current $g_\mu - 2$ experiment, we must still verify that it is possible to find specific functional forms $\delta\rho(w)$ which fit the μ -mesic X-ray discrepancy without seriously violating any of the conventional tests of QED, including the very high precision $g_e - 2$ and Lamb shift experiments.²¹ A postulated vacuum polarization discrepancy contributes to $g_e - 2$ through the diagram of Fig. 4(b), giving a formula identical to Eq. (27) apart from the replacement of m_μ in $f_a[t]$ by m_e . The smallness of m_e then permits use of the large- t asymptotic expression $\frac{1}{2}f_a \approx m_e^2/(3t)$, giving the simple expression

$$\begin{aligned} \delta a_e &\approx 0.60 \cdot 10^{-6} \int_{4m_e^2}^{\infty} \frac{dt}{t} \frac{m_e^2}{t} \delta\rho[t] \\ &= 0.15 \cdot 10^{-6} \int_0^{\infty} dw e^{-w} \delta\rho(w) \quad . \end{aligned} \tag{39}$$

Comparing Eq. (39) with the current difference between experiment and theory for a_e ,²²

$$a_e(\text{experiment}) - a_e(\text{conventional QED}) = (5.6 \pm 4.4) \cdot 10^{-9} \tag{40}$$

we get the restriction

$$\int_0^{\infty} dw e^{-w} \delta\rho(w) = (37 \pm 29) \cdot 10^{-3} \quad . \tag{41}$$

Next we consider the Lamb shift, which receives contributions from a vacuum polarization discrepancy via the diagram of Fig. 4(a). Working

again in the nonrelativistic hydrogenic approximation, we find for the change in the 2s - 2p Lamb transition energy

$$\begin{aligned} \delta \mathcal{L} \equiv \delta E_{2s \rightarrow 2p} &= \int_0^\infty r^2 dr [R_{20}(r)^2 - R_{21}(r)^2] \delta V(r) \\ &= -\frac{a_0 \alpha^2}{6\pi} \int_0^\infty \frac{dt \delta \rho[t]}{4m_e^2 \left(1 + t^{\frac{1}{2}} \frac{a_0}{Z}\right)^4} . \end{aligned} \quad (42)$$

Since $t^{\frac{1}{2}} a_0 Z^{-1} = (t^{\frac{1}{2}}/m_e) \alpha^{-1} Z^{-1} \gg 1$, we can neglect the 1 in the denominator of Eq. (38), giving

$$\delta \mathcal{L} = -\frac{Z^4 \alpha^5 m_e}{6\pi} \int_0^\infty \frac{dt}{4m_e^2} \frac{m_e^2}{t} \delta \rho[t] , \quad (43)$$

which evidently measures the same integral over $\delta \rho$ as does $g_e - 2$. It is easy to see that the formula for the $ns \rightarrow np$ Lamb transition is obtained by multiplying Eq. (43) by $(2/n)^3$. Hence, using the fact that

$$\frac{\alpha^5 m_e}{30\pi} \approx 27.1 \text{ MHz} , \quad (44)$$

we get the relation

$$\int_0^\infty dw e^{-w} \delta \rho(w) = \frac{n^3 [\mathcal{L}_{nZ}(\text{conventional QED}) - \mathcal{L}_{nZ}(\text{expt})]}{Z^4 \cdot 271 \text{ MHz}} . \quad (45)$$

In Table IV we have tabulated the right hand side of Eq. (45) for a series of measured Lamb transitions.²³ Taking a weighted average of the four best determinations [the two measurements for H(n=2) and the measurements for D(n=2) and He⁺(n=2)] we find

$$\int_0^{\infty} dw e^{-w} \delta\rho(w) = (0.29 \pm 1.0) \cdot 10^{-3}, \quad (46)$$

evidently a much tighter restriction than is obtained from $g_e - 2$.

Our procedure for searching for satisfactory functional forms $\delta\rho$ is now as follows. Let

$$\begin{aligned} \delta \bar{E}_Y(i), \sigma(i) &= \text{experimental reduced discrepancies and standard} \\ &\quad \text{deviations from Table II, } i=1, \dots, 12, \\ F(i) &= \text{theoretical fit to reduced discrepancies,} \\ &\quad i=1, \dots, 12; \\ \delta a_{\mu}^{\text{th}} &= \text{predicted change in } a_{\mu}, \\ \delta I^{\text{th}} &= \text{predicted value of } \int_0^{\infty} dw e^{-w} \delta\rho(w). \end{aligned} \quad (47)$$

We form two chi-squares,

$$\begin{aligned} \chi_1^2 &\equiv \sum_{i=1}^{12} \left[\frac{F(i) - \delta \bar{E}_Y(i)}{\sigma(i)} \right]^2, \\ \chi_2^2 &= \chi_1^2 + \left(\frac{\delta a_{\mu}^{\text{th}} - 2.6 \cdot 10^{-7}}{3.1 \cdot 10^{-7}} \right)^2 + \left(\frac{\delta I^{\text{th}} - 37 \cdot 10^{-3}}{29 \cdot 10^{-3}} \right)^2 \\ &\quad + \left(\frac{\delta I^{\text{th}} - 0.29 \cdot 10^{-3}}{1.0 \cdot 10^{-3}} \right)^2; \end{aligned} \quad (48)$$

the first tests the fit to the μ -mesic X-ray discrepancies alone, while the second tests the combined fit to the X-ray data and the $g_{\mu} - 2$, $g_e - 2$ and Lamb shift experiments. For each assumed functional form of $\delta\rho$, we treat the overall normalization as a free parameter and adjust it to

minimize either χ_1^2 or χ_2^2 , corresponding respectively to $12 - 1 = 11$ or $15 - 1 = 14$ degrees of freedom. A sampling of results of this procedure is shown in Tables V and VI. We conclude from these fits that:²⁴

(i) Functional forms giving good χ_2^2 fits can be found. When these same functional forms are fit by the χ_1^2 procedure the coefficients change by only about 25%, which is satisfactory.

(ii) The forms which give good χ_2^2 fits are all nearly step-function-like in character, with a turn-on at $w \approx 2 - 3$ [i.e., at $t \approx (30 - 80) m_e^2$]. The smallness below $w \sim 2$ is required by the Lamb shift data, while the slow growth above turn-on is needed in order not to violate the current limits on deviations in $g_\mu - 2$.

(iii) All of the good fits satisfy $\delta\rho \lesssim -0.03$ for large w . This is a general feature for any monotonic form $\delta\rho$ which is small in the Lamb-shift region $w \leq 2$, since (using the fact that $\bar{f}_Y \approx 0$ for $w \gtrsim 9$) we have

$$\begin{aligned}
 -54.5 \cdot 10^{-3} &= \int_0^\infty dw \bar{f}_Y(w) \delta\rho(w) \approx \int_2^9 dw \bar{f}_Y(w) \delta\rho(w) \\
 &\geq \delta\rho(9) \int_2^9 dw \bar{f}_Y(w) \\
 &= 1.6 \delta\rho(9) \quad ,
 \end{aligned}
 \tag{49}$$

that is

$$-0.034 \gtrsim \delta\rho(9) \quad .
 \tag{50}$$

Possible implications of Eq. (50) for QED tests involving time-like photon vertices will be discussed elsewhere.²⁵

One additional place where a vacuum polarization discrepancy should produce interesting effects is in the Lamb shift in muonic helium.²⁶ Applying Eq. (42) to this system (and noting that the 2p level here lies above the 2s level) we find

$$\begin{aligned} \delta \mathcal{L} ([^4\text{He}, \mu]^+) &\equiv \delta E_{2p \rightarrow 2s} = \frac{a_0 \alpha^2}{6\pi} \int_{\frac{2}{4m_e}}^{\infty} dt \frac{\delta \rho[t]}{\left(1+t^{\frac{1}{2}} \frac{a_0}{Z}\right)^4} \\ &= \frac{2}{3\pi} \alpha \frac{m_e^2}{m_\mu} \int_0^\infty dw f_{\text{He}}(w) \delta \rho(w) , \end{aligned} \quad (51)$$

$$f_{\text{He}}(w) = \frac{e^w}{\left(1 + \frac{m_e}{m_\mu \alpha} e^{w/2}\right)^4} , \quad f_{\text{He}}(0) \approx 0.13 .$$

Numerical evaluation of Eq. (51) shows that $f_{\text{He}}(w)/0.13$ lies within 20% of $\bar{f}_Y(w)$ in the range $0 \leq w \leq 6$ where neither is vanishingly small. Hence independent of the detailed form of $\delta \rho$, we find the prediction

$$\begin{aligned} \delta \mathcal{L} ([^4\text{He}, \mu]^+) &\sim \frac{2}{3\pi} \alpha \frac{m_e^2}{m_\mu} \times (-54.5 \cdot 10^{-3}) \times 0.13 \\ &\approx -0.027 \text{ eV} , \end{aligned} \quad (52)$$

which may be an observable effect.

At this point let us conclude our examination of vacuum polarization effects and turn to an alternative explanation for the μ -mesic X-ray discrepancy, the possible existence¹² of a weakly coupled scalar, isoscalar boson ϕ . Interest in this explanation has been stimulated by the fact that such particles (with undetermined mass) are called for in unified gauge

theories of the weak and electromagnetic interactions. Letting $g_{\phi\mu\bar{\mu}}$ and $g_{\phi NN}$ denote the ϕ -muon and the ϕ -nucleon scalar couplings, and M_ϕ the ϕ mass, the potential produced by ϕ -exchange between a muon and a nucleus of nucleon number A [Fig. 4(c)] is the simple Yukawa form²⁷

$$V_\phi(r) = - \frac{g_{\phi\mu\bar{\mu}} g_{\phi NN}}{4\pi} A \frac{e^{-M_\phi r}}{r} . \quad (53)$$

Since a repulsive potential is required to remove the X-ray discrepancy, fitting Eq. (53) to the X-ray data will necessarily give $g_{\phi\mu\bar{\mu}} g_{\phi NN} < 0$. As shown in Appendix C, this sign for the product of couplings is not possible in the simplest forms of gauge models, in which there is only one physical scalar meson and in which the chiral $SU(3) \otimes SU(3)$ symmetry breaking term in the strong interaction Lagrangian transforms as pure $(3, \bar{3}) \oplus (\bar{3}, 3)$. Nonetheless, let us proceed in a purely phenomenological fashion and make a quantitative fit of Eq. (53) to the X-ray data. Replacing $\delta V(r)$ in Eq. (22) by $V_\phi(r)$, we find

$$\delta\bar{E}'_Y \equiv \frac{\delta\bar{E}_Y}{\left(\frac{A}{2Z}\right)} = 2.82 \cdot 10^4 g_{\phi\mu\bar{\mu}} g_{\phi NN} f_Y [M_\phi^2] , \quad (54)$$

with $\delta\bar{E}'_Y$ the "reduced discrepancy" appropriate to a potential which couples to A rather than to Z . The experimentally measured values of $\delta\bar{E}'_Y$ are tabulated in Table VII. Since in all gauge models the ϕ -electron coupling is expected to be of order $(m_e/m_\mu) g_{\phi\mu\bar{\mu}}$, the ϕ will have a negligible effect on the electron $g_e - 2$ and Lamb shift measurements. So in fitting Eq. (54)

to the data we minimize χ_1^2 defined in Eq. (48), giving the results shown in Table VIII, in good agreement with the results quoted by Sundaresan and Watson.²⁸

Since a light scalar boson, as well as a vacuum polarization anomaly, can satisfactorily fit the X-ray discrepancy, let us examine ways of distinguishing between the two possible explanations. First we consider the muonic helium Lamb shift. Since $f_{\text{He}}(w) \approx \bar{f}_Y(w)$ for $0 \leq w \leq 6$, a scalar boson in the mass range from 1 to 22 MeV predicts an effect within about 20% of -0.027 eV, while for scalar bosons lighter than 1 MeV (corresponding to $w < 0$), the muonic helium Lamb shift decreases as

$$\delta \mathcal{L} ([^4\text{He}, \mu]^+) \sim \frac{-0.178 M_\phi^2}{(1 + 0.65 M_\phi)^4} \text{ eV}, \quad (55)$$

$$M_\phi \text{ in MeV}.$$

Hence the muonic helium experiment could only distinguish between a very light scalar boson²⁹ and the joint possibilities of a heavier scalar boson or a vacuum polarization effect. On the other hand, the muonic vertex correction involving scalar meson exchange makes a small positive²⁰ contribution to a_μ , as distinct from the sizeable negative contribution predicted by a vacuum polarization anomaly. So the next generation of $g_\mu - 2$ experiments should unambiguously distinguish between the vacuum polarization and scalar meson explanations for the μ -mesic atom X-ray discrepancy.

ACKNOWLEDGEMENTS

I wish to thank M. Baker, K. Johnson and above all S. Brodsky for conversations which stimulated the μ -mesic X-ray part of this paper. I have benefited from conversations with J. Bahcall, L. S. Brown, R. F. Dashen, B. Lautrup, B. W. Lee, J. Rafelski, V. Telegdi, S. B. Treiman, W. J. Weisberger, T. M. Yan, and A. Zee, and wish to thank S. B. Treiman for reading the manuscript.

Appendix A: Vector Meson Parameters

For the ω and ϕ vector meson parameters we take³⁰

$$\begin{aligned} M_\omega &= 784 \text{ MeV}, \quad \Gamma(\omega \rightarrow e^+ e^-) = 0.76 \text{ keV}, \\ M_\phi &= 1019 \text{ MeV}, \quad \Gamma(\phi \rightarrow e^+ e^-) = 1.36 \text{ keV}. \end{aligned} \quad (\text{A.1})$$

For $F_\pi(t)$ we use the Gounaris-Sakurai formula³¹ with an $\omega \rightarrow 2\pi$ interference term,³⁰

$$\begin{aligned} F_\pi(t) &= \frac{M_\rho^2 (1 + \delta \Gamma_\rho / M_\rho)}{M_\rho^2 - t + H(t) - i M_\rho \Gamma_\rho \left(\frac{k}{k_\rho}\right)^3 M_\rho / \sqrt{t}} + A e^{i\alpha} \frac{M_\omega^2}{M_\omega^2 - t - i M_\omega \Gamma_\omega}, \\ H(t) &= \frac{\Gamma_\rho M_\rho^2}{k_\rho^3} \left\{ k^2 [h(t) - h(M_\rho^2)] + k_\rho^2 h'(M_\rho^2) (M_\rho^2 - t) \right\}, \\ h(t) &= \frac{2}{\pi} \frac{k}{\sqrt{t}} \log \left(\frac{\sqrt{t} + 2k}{2m_\pi} \right), \\ h'(M_\rho^2) &= \frac{1}{2\pi M_\rho^2} + \frac{m_\pi^2}{\pi M_\rho^3 k_\rho} \log \left(\frac{M_\rho + 2k_\rho}{2m_\pi} \right), \\ k &= \left(\frac{1}{4} t - m_\pi^2 \right)^{\frac{1}{2}}, \quad k_\rho = \left(\frac{1}{4} M_\rho^2 - m_\pi^2 \right)^{\frac{1}{2}}, \\ A &= \frac{6 B^{\frac{1}{2}}(\omega \rightarrow ee) \Gamma_\omega}{\alpha M_\omega \beta_\pi^{3/2}} B^{\frac{1}{2}}(\omega \rightarrow 2\pi), \\ \beta_\pi &= \left(1 - \frac{4m_\pi^2}{t} \right)^{\frac{1}{2}}, \end{aligned} \quad (\text{A.2})$$

with the following values for the parameters,³⁰

$$\begin{aligned} \delta &= 0.6, & \alpha &= 86^\circ, \\ M_\rho &= 775 \text{ MeV}, & \Gamma_\omega &= 9.2 \text{ MeV}, \\ \Gamma_\rho &= 149 \text{ MeV}, & B^{\frac{1}{2}}(\omega \rightarrow ee) &= 0.906 \cdot 10^{-2}, \\ m_\pi &= 140 \text{ MeV}, & B^{\frac{1}{2}}(\omega \rightarrow 2\pi) &= 0.19. \end{aligned} \tag{A.3}$$

As discussed in Appendix B, approximating the small- t region in this fashion as a sum of ω , ϕ and ρ contributions should yield the small- t contribution to $T_{\text{obs}}(-s)$ (which is only a small fraction of the total for large $-s$) to an accuracy of about 15%.

Appendix B:

Formulas for $f_a[t]$ and the Hadronic Contribution to $g_{\mu} - 2$

The function $f_a[t]$ appearing in Eq. (27) has been evaluated by Brodsky and de Rafael,³² who find

$$\begin{aligned}
 f_a[t] &\equiv 2K(t) , \\
 0 \leq t &\leq 4m_{\mu}^2 \quad \tau = t/4m_{\mu}^2 , \\
 K(t) &= \frac{1}{2} - 4\tau - 4\tau(1-2\tau) \ln(4\tau) \\
 &\quad - 2(1-8\tau+8\tau^2) \left(\frac{\tau}{1-\tau}\right)^{\frac{1}{2}} \arctan\left(\frac{1-\tau}{\tau}\right)^{\frac{1}{2}} ; \\
 t \geq 4m_{\mu}^2 , \quad x &= \frac{1 - (1-4m_{\mu}^2/t)^{\frac{1}{2}}}{1 + (1-4m_{\mu}^2/t)^{\frac{1}{2}}} , \\
 K(t) &= \frac{1}{2} x^2(2-x^2) + (1+x)^2(1+x^2) \cdot \frac{\ln(1+x) - x + \frac{1}{2}x^2}{x^2} + \frac{1+x}{1-x} x^2 \ln x .
 \end{aligned} \tag{B.1}$$

Corresponding to the division of $T_{\text{obs}}(-s)$ into four pieces in Eq. (15), we write the hadronic contribution to a_{μ} as

$$\begin{aligned}
 a_{\mu} &= \frac{1}{4\pi^3} \int_{4m_{\pi}^2}^{\infty} dt \sigma(e^+e^- \rightarrow \text{hadrons}; t) K(t) \\
 &= a_{\mu}^{\omega+\phi} + a_{\mu}^{\rho} + a_{\mu}^{\text{cont}(1)} + a_{\mu}^{\text{cont}(2)} .
 \end{aligned} \tag{B.2}$$

Working in the same narrow resonance approximation as in the text we find

for $a_{\mu}^{\omega+\phi}$ the expression⁶

$$a_{\mu}^{\omega+\phi} = \sum_{V=\omega, \phi} \frac{3}{\pi} K(M_V^2) \frac{\Gamma(V \rightarrow e^+e^-)}{M_V} , \tag{B.3}$$

while a_{μ}^{ρ} is given by the integral

$$a_{\mu}^{\rho} = \frac{\alpha^2}{12\pi^2} \int_{4m_{\pi}^2}^{\infty} \frac{dt}{t} \left(1 - \frac{4m_{\pi}^2}{t} \right)^{3/2} |F_{\pi}(t)|^2 K(t) . \quad (\text{B. 4})$$

Substituting the parameters from Appendix A and evaluating Eq. (B. 3) and (B. 4) numerically gives

$$\begin{aligned} a_{\mu}^{\omega+\phi} &= 9.1 \cdot 10^{-9} , & a_{\mu}^{\rho} &= 45 \cdot 10^{-9} , \\ a_{\mu}^{\text{tot. small-t}} &= 54 \cdot 10^{-9} . \end{aligned} \quad (\text{B. 5})$$

A more elaborate evaluation of the small-t contribution has been given by Bramòn, Etim and Greco,³³ who sum the contributions of the various important hadronic states directly from Eq. (B. 2), giving

$$a_{\mu}^{\text{tot. small-t}} = (61 \pm 7) \cdot 10^{-9} , \quad (\text{B. 6})$$

indicating that our method of treating the small-t region is good to about 15%. To evaluate $a_{\mu}^{\text{cont}(1)}$ and $a_{\mu}^{\text{cont}(2)}$ we approximate $K(t)$ by its asymptotic form

$$K(t) \approx \frac{1}{3} \frac{m_{\mu}^2}{t} \quad t \rightarrow \infty , \quad (\text{B. 7})$$

giving [in units where unity = $(1 \text{ GeV}/c)^2$]

$$\begin{aligned} a_{\mu}^{\text{cont}(1)} &= 6.7 \cdot 10^{-9} \int_{0.39}^{25} \frac{dt R(t)}{t^2} , \\ a_{\mu}^{\text{cont}(2)} &= 6.7 \cdot 10^{-9} \int_{25}^{t_C} \frac{dt R(t)}{t^2} . \end{aligned} \quad (\text{B. 8})$$

Evaluating $a_{\mu}^{\text{cont}(1)}$ numerically using the data plotted in Fig. 1 gives

$$a_{\mu}^{\text{cont}(1)} = 9.6 \pm 2 , \quad (\text{B. 9})$$

with the error a rough guess. Thus the total known hadronic contribution to a_{μ} is

$$(61 \pm 7) \cdot 10^{-9} + (9.6 \pm 2) \cdot 10^{-9} = (71 \pm 7) \cdot 10^{-9}. \quad (\text{B.10})$$

Estimating the unmeasured contribution by assuming a linearly rising $R(t)$ up to $t_C = (2.230)^2$, we get

$$a_{\mu}^{\text{cont}(2)} = 6.7 \cdot 10^{-9} \times 0.24 \ln \frac{(460)^2}{25} = 15 \cdot 10^{-9}, \quad (\text{B.11})$$

as stated in the text.

Appendix C:

Sign of the Scalar Meson Exchange Potential in Simple Gauge Theories.

Consider a gauge theory of the weak and electromagnetic interactions in which only one scalar field ϕ develops a vacuum expectation, $\phi \rightarrow \phi + \lambda$, as a result of spontaneous symmetry breaking. Since λ is the source of the lepton masses, the interaction Hamiltonian (= - the interaction Lagrangian) coupling ϕ to the muons is³⁴

$$\mathcal{H}_{\phi\mu\bar{\mu}} = \frac{\phi}{\lambda} m_{\mu} \bar{\psi}_{\mu} \psi_{\mu} . \quad (C.1)$$

Since in the hadronic sector λ is the origin of chiral $SU(3) \otimes SU(3)$ symmetry breaking, the interaction Hamiltonian coupling ϕ to the hadrons is³⁴

$$\mathcal{H}_{\phi \text{ hadron}} = \frac{\phi}{\lambda} \delta \mathcal{H}_{\text{chiral breaking}} . \quad (C.2)$$

Hence the sign of $g_{\phi\mu\bar{\mu}} g_{\phi NN}$ is the same as the sign of $\langle N | \delta \mathcal{H}_{\text{chiral breaking}} | N \rangle$. Now if $\delta \mathcal{H}_{\text{chiral breaking}}$ transforms under $SU(3) \otimes SU(3)$ as $(3, \bar{3}) \oplus (\bar{3}, 3)$, then using the notation of Gell-Mann, Oakes, and Renner³⁵ we readily find that

$$\langle N | \delta \mathcal{H}_{\text{chiral breaking}} | N \rangle = \frac{3 \sigma_{\pi NN}}{(\sqrt{2} + c)\sqrt{2}} + (c - \frac{1}{\sqrt{2}}) \langle N | u_8 | N \rangle ,$$

$$c \approx \sqrt{2} \frac{m_K^2 - m_{\pi}^2}{m_K^2 + \frac{1}{2} m_{\pi}^2} = -1.25 , \quad (C.3)$$

$$\langle N | u_8 | N \rangle = \text{baryon mass splitting parameter} = 170 \text{ MeV} ,$$

$$\sigma_{\pi NN} \equiv \frac{1}{3} (\sqrt{2} + c) \langle N | \sqrt{2} u_0 + u_8 | N \rangle .$$

That is, we have

$$\langle N | \delta \text{chiral breaking} | N \rangle = 12.9 \sigma_{\pi NN} - 333 \text{ MeV} . \quad (\text{C. 4})$$

Recent determinations of the sigma term $\sigma_{\pi NN}$ suggest a value in the range 45 - 85 MeV,³⁶ making $\langle N | \delta \text{chiral breaking} | N \rangle$ positive and giving an attractive scalar meson exchange force. A value of $\sigma_{\pi NN}$ smaller than 25 MeV would be needed to make the scalar meson exchange force repulsive, as is required to explain the μ -mesic X-ray discrepancy.

REFERENCES

1. For a summary of the recent data, see R. Gatto and G. Preparata, CERN TH.1852, 1974 (unpublished).
2. A good review of the relevant experiments and theory is given by P. J. S. Watson and M. K. Sundaresan, Discrepancy between Theory and Experiments in Muonic X-rays - a Critical Discussion, Carleton University preprint.
3. L. Silvestrini, Electron-Positron Interactions, in Proceedings of the XVI International Conference on High Energy Physics, Chicago - Batavia, 1972, V4, p. 1.
4. T. Appelquist and H. Georgi, Phys. Rev. D8, 4000 (1973); A. Zee, Phys. Rev. D8, 4038 (1973).
5. See, for example, C. H. Llewellyn Smith, CERN TH. 1849, 1974 (unpublished); N. Cabibbo and G. Karl, CERN TH. 1858, 1974 (unpublished).
6. We follow the treatment of the vector meson contributions to $\sigma(e^+e^- \rightarrow \text{hadrons}; t)$ given by M. Gourdin and E. de Rafael, Nuclear Physics B10, 667 (1969).
7. J. Arafune, Phys. Rev. Letters 32, 560 (1974); L. S. Brown, R. N. Cahn and L. D. McLerran, Phys. Rev. Letters 32, 562 (1974); M. Gyulassy, Phys. Rev. Letters 32, 1393 (1974).
8. J. Rafelski, B. Müller, G. Soff and W. Greiner, Critical Discussion of the Vacuum Polarization Measurements in Muonic Atoms, Univ. of Penn. preprint.

9. M. S. Dixit, H. L. Anderson, et al., Phys. Rev. Letters 27, 878 (1971).
10. H. Walter, J. W. Vuilleumier, et al., Phys. Letters 40B, 197 (1972).
11. S. L. Adler, Phys. Rev. D5, 3021 (1972); K. Johnson and M. Baker, Phys. Rev. D8, 1110 (1973).
12. M. K. Sundaesan and P. J. S. Watson, Phys. Rev. Letters 29, 15 (1972); L. Resnick, M. K. Sundaesan and P. J. S. Watson, Phys. Rev. D8, 172 (1973).
13. To make the definition of $\delta\rho$ precise, we are assuming $\delta\rho$ to be an extra contribution to the vacuum polarization two-point spectral function above and beyond the usual second and fourth order electron and muon contributions, of a magnitude much larger than the naive perturbative estimate of the sixth and higher order terms. Because $Z\alpha$ is not a very small parameter for some of the atomic species being considered, in establishing the existence of the μ -mesic anomaly it is important to take into account 4, 6, ...-point vacuum polarization amplitudes in which one vertex emits a photon coupling to the muon and all the remaining vertices couple to the nuclear Coulomb potential. Numerically, the contribution of such diagrams to the X-ray energies is only a few percent of the Uehling potential contribution, so we neglect possible nonperturbative modifications of the higher point functions.
14. Just to set the energy scale involved, the Uehling energies are typically 0.2 - 3 keV out of total transition energies of 150 - 500 keV.

15. We assume independence of errors and add errors in quadrature for both the μ -mesic discrepancies and the Lamb shift measurements. If systematic errors are large, then the errors for average quantities will be larger than those quoted, making the constraints on the χ^2 fits less restrictive than those we have assumed.
16. B. Lautrup, A. Peterman and E. deRafael, *Physics Reports* 3C, 193 (1972).
17. V. W. Hughes, Status of QED Experiments, in S. J. Smith and G. K. Walters, eds., Atomic Physics 3, Plenum Press, N. Y., 1973, p. 1; B. Lautrup (unpublished).
18. B. Lautrup, *Phys. Letters* 38B, 408 (1972); M. A. Samuel, *Phys. Rev. D* (in press).
19. C. H. Llewellyn Smith, Ref. 5; N. Cabibbo and R. Gatto, *Phys. Rev.* 124, 1577 (1961).
20. R. Jackiw and S. Weinberg, *Phys. Rev.* D5, 2396 (1972); I. Bars and M. Yoshimura, *Phys. Rev.* D6, 374 (1972); J. R. Primack and H. R. Quinn, *Phys. Rev.* D6, 3171 (1972).
21. The atomic fermium K_{α} X-ray measurements of P. F. Dittner et al., *Phys. Rev. Letters* 26, 103 (1971) only probe the Uehling potential to an accuracy of about 20%. See B. Fricke et al., *Phys. Rev. Letters* 28, 714 (1972). Constraints imposed by time-like photon vertex measurements are discussed in S. J. Adler, R. F. Dashen, and S. B. Treiman (Institute for Advanced Study preprint).
22. N. M. Kroll, Status of Quantum Electrodynamics Theory, in S. J. Smith and G. K. Walters, eds., Atomic Physics 3, Plenum Press, N. Y., 1973, p. 33.

23. The data are taken from Ref. 16, except for L_1^{++} , where we use the more accurate measurements of P. Leventhal and P.G. Havey, Phys. Rev. Letters 32, 808 (1974).
24. The conclusion that satisfactory fits can be found has also been reached by F. Heile (SLAC, unpublished), using a momentum space parameterization of the vacuum polarization discrepancy.
25. S. L. Adler, R. F. Dashen, and S. B. Treiman (in preparation). We show in this paper that a decrease in the vacuum polarization spectral function necessarily implies a decrease in the vertex for emission of a time-like photon, and tests of the effect are suggested. Obviously, modifications in vertex parts will at some level make contributions to the electrodynamic processes discussed in the present paper above and beyond the direct effect of the postulated vacuum polarization discrepancy. There seems at present to be no way of estimating the size of such additional contributions; about all one can say is that they are likely to be most important in the electron Lamb shift and $g_e - 2$ experiments, where only one mass scale (m_e) is involved and the vacuum polarization and photon-electron vertex parts are off-shell to a similar degree. Hence the electronic Lamb shift predictions of Tables V and VI should not be taken too literally. On the other hand, in the muon energy level and $g_\mu - 2$ experiments, two mass scales (both m_e and m_μ) are involved, with the electron vacuum polarization loops much further off shell (relative to their natural mass scale) than are the photon-muon vertices. Thus in this case the neglect of possible vertex modifications, which is implicit in all of the discussion of the text, may well be justified.
26. E. Campini, Lettere al Nuovo Cimento 4, 982 (1970); P. J. S. Watson and M. K. Sundaresan, Ref. 2.

27. The factor $(4\pi)^{-1}$ in Eq. (49) appears to have been omitted in the basic paper of R. Jackiw and S. Weinberg, Phys. Rev. D5, 2396 (1972) and in subsequent papers quoting their formulas.
28. Because of the factor of 4π mentioned in Ref. 26, our $(g_{\phi\mu\bar{\mu}} g_{\phi NN})/4\pi$ should be compared with $g_{\phi\mu\bar{\mu}} g_{\phi NN}$ of Ref. 2. Omitting the ^{20}Ca , ^{22}Ti , ^{26}Fe and ^{38}Sr discrepancies from the fit, as was done in Ref. 2, we find an effective coupling of $-7.6 \cdot 10^{-7}$ at $M_\phi = 12$ MeV, in agreement with the magnitude of $8.0 \cdot 10^{-7}$ quoted in Ref. 2. The numerical results of Table VIII were obtained by fitting to all discrepancy data.
29. The possibility of a very light scalar meson may well be almost academic. An experiment reported by D. Kohler, J. A. Becker, and B. A. Watson [Bull. Am. Phys. Soc. Series II V19 #4, 514 (1974)] looks, via the e^+e^- decay mode, for a ϕ produced in the transition from the $^{16}\text{O}(6.05 \text{ MeV})$ and $^4\text{He}(20.2 \text{ MeV}) 0^+$ states to the 0^+ ground states, and concludes that M_ϕ cannot be between 1.030 MeV and 18 MeV. Furthermore, neutron electron scattering data rule out $M_\phi \lesssim 0.6$ MeV (see Ref. 24), leaving only a narrow allowed region between 0.6 and 1.03 MeV! These remarks do not apply to the derivative coupled ϕ discussed recently by S. Barshay (to be published), where the electron coupling is smaller than the μ coupling by two, as opposed to one, powers of m_e/m_μ .
30. The data used are taken from J. Lefrancois, Results of the Orsay Storage Ring A. C. O., Proceedings of the 1971 International Symposium on Electron and Photon Interactions at High Energies, Cornell, 1971, p. 51.
31. G. J. Gounaris and J. J. Sakurai, Phys. Rev. Letters 21, 244 (1968).
32. S. J. Brodsky and E. de Rafael, Phys. Rev. 168, 1620 (1968) and Phys. Rev. 174, 1835 (1968).

33. A. Bramón, E. Etim, and M. Greco, Phys. Letters 39B, 514 (1972).
34. R. Jackiw and S. Weinberg, Ref. 20.
35. M. Gell-Mann, R. J. Oakes, and B. Renner, Phys. Rev. 175, 2195 (1968). See also B. Renner, On the Problem of the Sigma Terms in Meson-Baryon Scattering - Comments on Recent Literature, in Springer Tracts in Modern Physics, V. 61, p. 121.
36. H. Pilkuhn et al., Nuclear Physics B65, 460 (1973). See especially pp. 480 - 481. The estimate of Eq. (C.4) is also given by E. Reya, Chiral Symmetry Breaking and Meson-Nucleon Sigma Commentators: A Review, Reviews of Modern Physics (in press). Reya writes $M_B = M_0 + \langle B | \delta \text{chiral breaking} | B \rangle$, where M_0 is the baryon mass in the absence of $SU(3) \otimes SU(3)$ breaking. For the $(3, \bar{3}) \oplus (\bar{3}, 3)$ case, he finds $M_0 = 1300 \text{ MeV} - 13\sigma_{\pi NN}$, so for $\sigma_{\pi NN}$ in the range 45-85 MeV the mass M_0 is less than the nucleon mass, making $\langle N | \delta \text{chiral breaking} | N \rangle$ positive.

TABLE I.

Values of C in Different Models

<u>Model</u>	<u>C</u>
Simple quark triplet	2/3
Color quark triplet	2
Color quark quartet	10/3
Han-Nambu triplet	4
Han-Nambu quartet	6

TABLE II.

Muonic Atom X-ray Discrepancies

Element Z	Transition $n_l - n - 1 \rightarrow j - 1$	E_Y (th) - E_Y (expt) (eV)	Average Discrepancy - δE_Y (eV)	Reduced Average Discrepancy $-\delta \bar{E}_Y = \frac{-\delta E_Y}{4.35 \text{ eV } Z^2 \left[\frac{1}{(n-1)^2} - \frac{1}{n^2} \right]}$
^{20}Ca	$^3d_{3/2} - ^2p_{1/2}$	7 ± 19	9 ± 13	$(37.2 \pm 54) \cdot 10^{-3}$
	$^3d_{5/2} - ^2p_{3/2}$	11 ± 17		
^{22}Ti	$^3d_{3/2} - ^2p_{1/2}$	-3 ± 19	3.5 ± 13	$(12.0 \pm 45) \cdot 10^{-3}$
	$^3d_{5/2} - ^2p_{3/2}$	10 ± 18		
^{26}Fe	$^3d_{3/2} - ^2p_{1/2}$	21 ± 20	15.5 ± 13	$(37.9 \pm 32) \cdot 10^{-3}$
	$^3d_{5/2} - ^2p_{3/2}$	10 ± 17		
^{38}Sr	$^4f_{5/2} - ^3d_{3/2}$	11 ± 20	5.5 ± 13	$(18.0 \pm 43) \cdot 10^{-3}$
	$^4f_{7/2} - ^3d_{5/2}$	0 ± 18		
^{47}Ag	$^4f_{5/2} - ^3d_{3/2}$	27 ± 20	23 ± 14	$(49.3 \pm 30) \cdot 10^{-3}$
	$^4f_{7/2} - ^3d_{5/2}$	19 ± 20		
^{48}Cd	$^4f_{5/2} - ^3d_{3/2}$	13 ± 19	10 ± 13	$(20.5 \pm 27) \cdot 10^{-3}$
	$^4f_{7/2} - ^3d_{5/2}$	7 ± 17		

TABLE II. - CONTINUED
Muonic Atom X-ray Discrepancies

Element Z^E	Transition $n_l j \rightarrow n-1 l-1 j-1$	$E_Y(\text{th}) - E_Y(\text{expt})$ (eV)	Average Discrepancy $-\delta E_Y$ (eV)	Reduced Average Discrepancy $-\delta \bar{E}_Y = \frac{-\delta E_Y}{4.35 \text{eV } Z^2} \left[\frac{1}{(n-1)^2} - \frac{1}{n^2} \right]$
^{50}Sn	$4f_{5/2} \rightarrow 3d_{3/2}$	21 ± 21	23 ± 14	$(43.5 \pm 26) \cdot 10^{-3}$
	$4f_{7/2} \rightarrow 3d_{5/2}$	25 ± 19		
^{56}Ba	$4f_{5/2} \rightarrow 3d_{3/2}$	55 ± 23	65.5 ± 15	$(98.8 \pm 23) \cdot 10^{-3}$
	$4f_{7/2} \rightarrow 3d_{5/2}$	76 ± 20		
	$5g_{7/2} \rightarrow 4f_{5/2}$	12 ± 17		
	$5g_{9/2} \rightarrow 4f_{7/2}$	3 ± 16		
^{80}Hg	$5g_{7/2} \rightarrow 4f_{5/2}$	52 ± 24	45 ± 17	$(71.8 \pm 27) \cdot 10^{-3}$
	$5g_{9/2} \rightarrow 4f_{7/2}$	38 ± 25		
^{81}Tl	$5g_{7/2} \rightarrow 4f_{5/2}$	31 ± 24	35.5 ± 17	$(55.3 \pm 26) \cdot 10^{-3}$
	$5g_{9/2} \rightarrow 4f_{7/2}$	40 ± 24		
^{82}Pb	$5g_{7/2} \rightarrow 4f_{5/2}$	52 ± 21	48.5 ± 14	$(73.7 \pm 21) \cdot 10^{-3}$
	$5g_{9/2} \rightarrow 4f_{7/2}$	45 ± 18		

TABLE III.

Transitions with Nearly Identical f_{γ}

<u>Element</u> <u>Z^E</u>	<u>Transition</u> <u>$n_l \rightarrow n_{l-1}$</u>	<u>Reduced Average</u> <u>Discrepancy $-\delta \bar{E}_{\gamma}$</u>
47 ^{Ag}	$4_f \rightarrow 3_d$	$(49.3 \pm 30) \cdot 10^{-3}$
48 ^{Cd}	$4_f \rightarrow 3_d$	$(20.5 \pm 27) \cdot 10^{-3}$
50 ^{Sn}	$4_f \rightarrow 3_d$	$(43.5 \pm 26) \cdot 10^{-3}$
80 ^{Hg}	$5_g \rightarrow 4_f$	$(71.8 \pm 27) \cdot 10^{-3}$
81 ^{Tl}	$5_g \rightarrow 4_f$	$(55.3 \pm 26) \cdot 10^{-3}$
82 ^{Pb}	$5_g \rightarrow 4_f$	$(73.7 \pm 21) \cdot 10^{-3}$
Weighted average of six reduced discrepancies ^a :		<u>$(54.5 \pm 10) \cdot 10^{-3}$</u>

a

We have treated the errors as if they were purely statistical and quoted the RMS error for the average.

TABLE IV.
Lamb Shift Measurements

<u>System</u>	<u>Conventional QED (MHz)</u>	<u>Expt (MHz)</u>	<u>Right-hand Side of Eq. (41)</u>
H(n = 2)	1057.911 ± 0.012	1057.90 ± 0.06	(0.33 ± 1.80) · 10 ⁻³
		1057.86 ± 0.06	(1.50 ± 1.80) · 10 ⁻³
H(n = 3)	314.896 ± 0.003	314.810 ± 0.052	(8.57 ± 5.18) · 10 ⁻³
H(n = 4)	133.084 ± 0.001	133.18 ± 0.59	(-22.7 ± 139) · 10 ⁻³
D(n = 2)	1059.271 ± 0.025	1059.28 ± 0.06	(-0.27 ± 1.92) · 10 ⁻³
He ⁺ (n = 2)	14044.765 ± 0.613	14045.4 ± 1.2	(-1.18 ± 2.49) · 10 ⁻³
He ⁺ (n = 3)	4184.42 ± 0.18	4183.17 ± 0.54	(7.79 ± 3.55) · 10 ⁻³
He ⁺ (n = 4)	1769.088 ± 0.076	1769.4 ± 1.2	(-4.60 ± 17.7) · 10 ⁻³
Li ⁺⁺ (n = 2)	62762 ± 9	62765 ± 21	(-1.1 ± 8.3) · 10 ⁻³
C ⁵⁺ (n = 2)	(783.678 ± 0.251) · 10 ⁻³	(744.0 ± 7) · 10 ⁻³	(904 ± 159) · 10 ⁻³

TABLE V.

Sample Functional Forms Giving Statistically Satisfactory Fits

(1) Fits minimizing χ_2^2		χ_2^2	$\delta a \cdot 10^7$	$\delta \mathcal{L} \text{ (H) MHz}^a$
Functional Form	$\delta \rho(w)$			
-0.053 $\theta(w-3)$		12.1	-1.9	0.08
-0.071 $\left(\frac{w-3}{w}\right)^{0.2} \theta(w-3)$		12.1	-2.1	0.08
-0.16 $\left(\frac{w-2}{w}\right)^2 \theta(w-2)$		12.9	-2.4	0.08
(2) Fits minimizing χ_1^2		χ_1^2	$\delta a \cdot 10^7$	$\delta \mathcal{L} \text{ (H) MHz}^a$
Functional Form	$\delta \rho(w)$			
-0.066 $\theta(w-3)$		7.9	-2.3	0.10
-0.088 $\left(\frac{w-2}{w_2}\right)^{0.2} \theta(w-3)$		7.9	-2.6	0.10
-0.21 $\left(\frac{w-2}{w}\right)^2 \theta(w-2)$		8.1	-3.1	0.11
(3) Reduced discrepancies predicted by the fit $-0.071 \left(\frac{w-3}{w}\right)^{0.2} \theta(w-3)$				
Z	20 22 26 38 47 48 50 56 56 80 81 82			
Transition $n \rightarrow n-1$	3 \rightarrow 2 3 \rightarrow 2 3 \rightarrow 2 4 \rightarrow 3 5 \rightarrow 4 5 \rightarrow 4 5 \rightarrow 4			
$-10^3 \cdot \delta \bar{E}_\gamma$ (expt)	37.2 12.0 37.9 18.0 49.3 20.5 43.5 98.8 24.4 71.8 55.3 73.7			
	± 54 ± 45 ± 32 ± 43 ± 30 ± 27 ± 26 ± 23 ± 39 ± 27 ± 26 ± 21			
$-10^3 \cdot \delta \bar{E}_\gamma$ (fit)	40.6 46.2 57.3 30.5 42.5 43.8 46.5 54.2 21.6 40.0 40.8 41.6			

^a See the comment in Ref. 25.

TABLE VI.

Results of Step Function Fits

<u>Functional Form $\delta\rho$</u>	<u>χ^2_2</u>	<u>$\delta a_\mu \cdot 10^7$</u>	<u>$\delta A (H) \text{ MHz}^a$</u>
-0.004 $\theta(w - 0.5)$	38	-0.23	0.08
-0.014 $\theta(w - 1.5)$	21	-0.69	0.10
-0.032 $\theta(w - 2.5)$	14	-1.3	0.09
-0.072 $\theta(w - 3.5)$	12	-2.3	0.07
-0.16 $\theta(w - 4.5)$	13	-4.0	0.06
-0.37 $\theta(w - 5.5)$	22	-6.7	0.05
-0.39 $\theta(w - 6.5)$	43	-5.0	0.02

^a See the comment in Ref. 25.

TABLE VII.

Reduced Discrepancies for Scalar Meson Calculation

Element Z^E	Transition $n_\ell \rightarrow n-1_{\ell-1}$	Reduced Average Discrepancy $-\delta\bar{E}_Y'$
20^{Ca}	$3d \rightarrow 2p$	$(37.2 \pm 54) \cdot 10^{-3}$
22^{Ti}	$3d \rightarrow 2p$	$(11.0 \pm 41) \cdot 10^{-3}$
26^{Fe}	$3d \rightarrow 2p$	$(35.1 \pm 30) \cdot 10^{-3}$
38^{Sr}	$4f \rightarrow 3d$	$(15.5 \pm 37) \cdot 10^{-3}$
47^{Ag}	$4f \rightarrow 3d$	$(42.9 \pm 26) \cdot 10^{-3}$
48^{Cd}	$4f \rightarrow 3d$	$(17.5 \pm 23) \cdot 10^{-3}$
50^{Sn}	$4f \rightarrow 3d$	$(36.6 \pm 22) \cdot 10^{-3}$
56^{Ba}	$4f \rightarrow 3d$	$(81.0 \pm 19) \cdot 10^{-3}$
	$5g \rightarrow 4f$	$(20.0 \pm 32) \cdot 10^{-3}$
80^{Hg}	$5g \rightarrow 4f$	$(57.0 \pm 21) \cdot 10^{-3}$
81^{Tl}	$5g \rightarrow 4f$	$(43.9 \pm 21) \cdot 10^{-3}$
82^{Pb}	$5g \rightarrow 4f$	$(58.5 \pm 17) \cdot 10^{-3}$

TABLE VIII.

Results of Scalar Meson Fits

<u>M_ϕ (MeV)</u>	<u>χ_1^2</u>	<u>$(g_{\phi\mu\mu} - g_{\phi N\bar{N}}) / 4\pi$</u>
0.5	8.1	$-1.3 \cdot 10^{-7}$
1	7.9	$-1.4 \cdot 10^{-7}$
4	6.8	$-2.0 \cdot 10^{-7}$
8	6.1	$-3.8 \cdot 10^{-7}$
12	6.5	$-6.9 \cdot 10^{-7}$
16	7.5	$-1.2 \cdot 10^{-6}$
22	10.1	$-2.5 \cdot 10^{-6}$

FIGURE CAPTIONS

- Fig. 1 "Eyeball" fit to the continuum e^+e^- annihilation data. The ρ , ω , and ϕ vector meson contributions are not included.
- Fig. 2 The function $T_{\text{obs}}(-s)$ as obtained from all experimental data up to $t_c = 25 (\text{GeV}/c)^2$, in units where unity = $(1 \text{ GeV}/c)^2$.
- Fig. 3 Ratios of $T_{\text{obs}}(-s)$ to $T_{\text{th}}(-s)$, with $T_{\text{th}}(-s)$ the color triplet prediction of Eq. (13). The $t_c = 25$ curve uses the presently known data; the curves for higher t_c assume a constant hadronic annihilation cross section of $21 \cdot 10^{-33} \text{ cm}^2$ above $25 (\text{GeV}/c)^2$.
- Fig. 4 (a) Diagram by which a vacuum polarization modification (denoted by the shaded blob) contributes to μ - and e - atomic energy levels.
- (b) Diagram by which a vacuum polarization modification contributes to $g_\mu - 2$ and $g_e - 2$.
- (c) Diagram by which a scalar meson contributes to μ - atomic energy levels.
- (d) Diagram by which a scalar meson contributes to $g_\mu - 2$.
- Fig. 5 Kernels f_γ for some representative transitions.
- Fig. 6 Plots of the kernels \bar{f}_γ and f_{ar} [see the discussion which follows Eqs. (28) and (29) of the text].

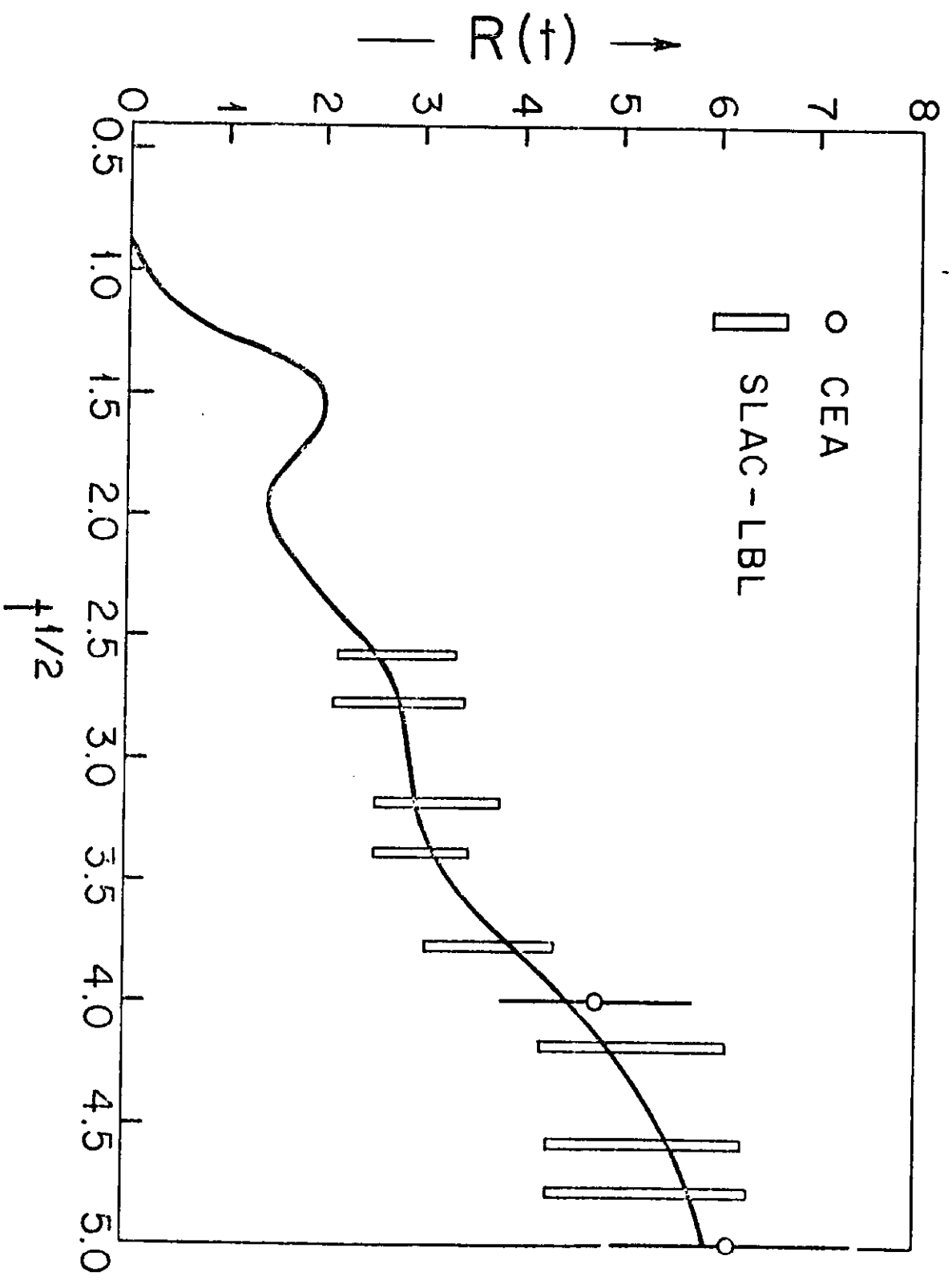


FIG. 1

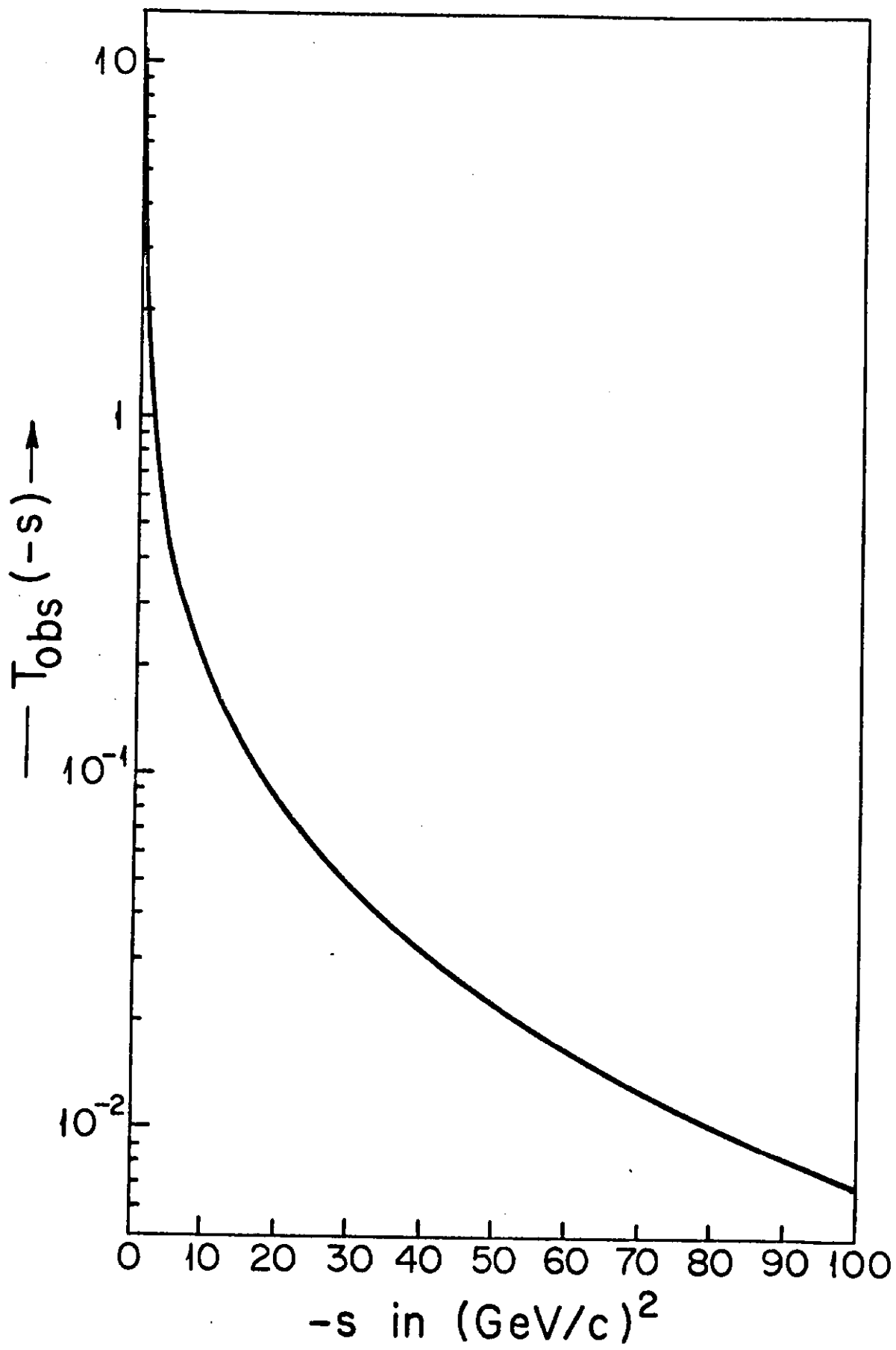
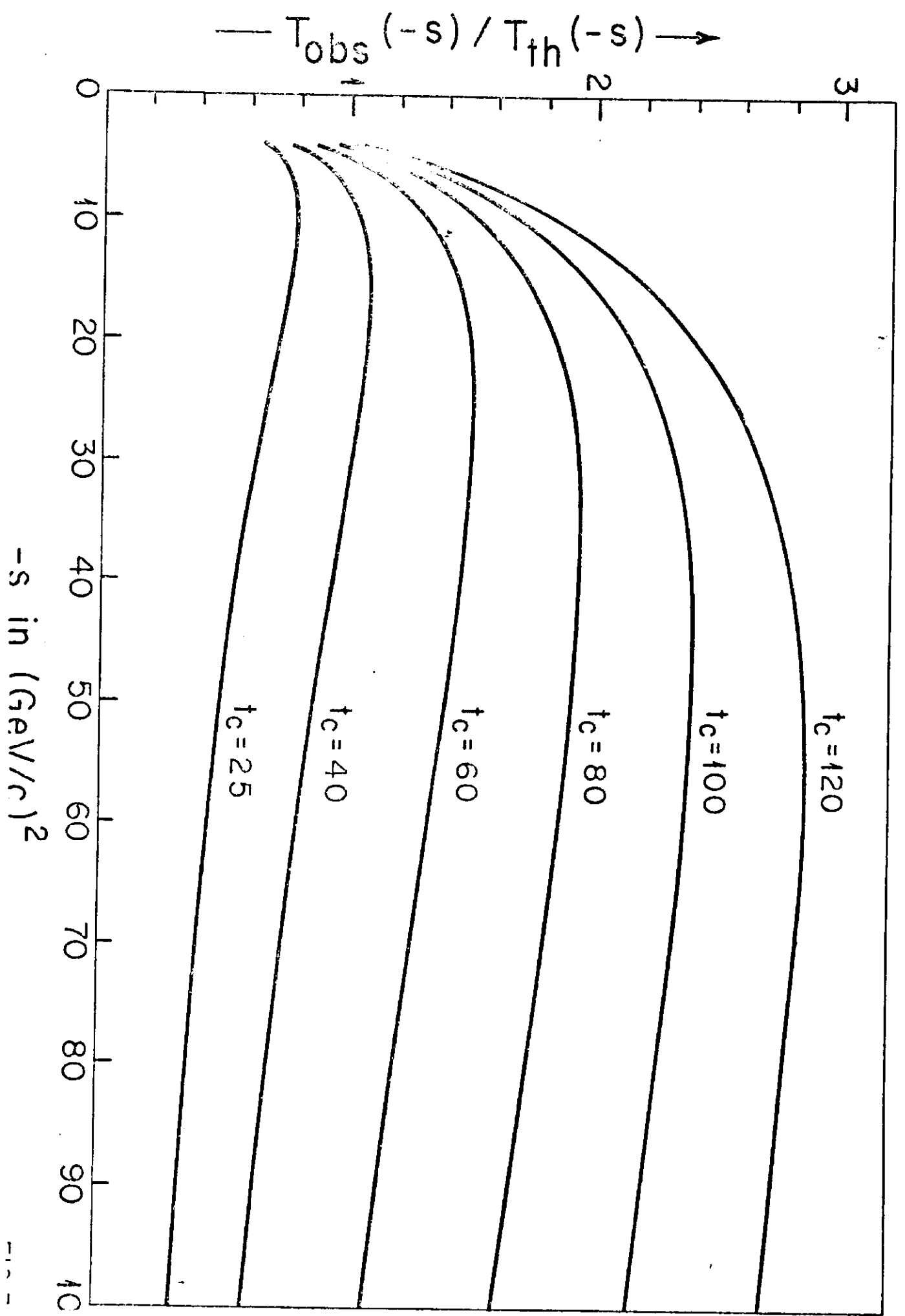
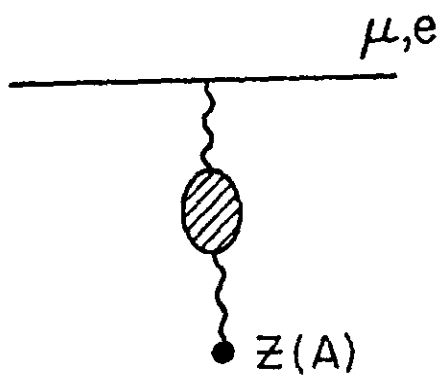
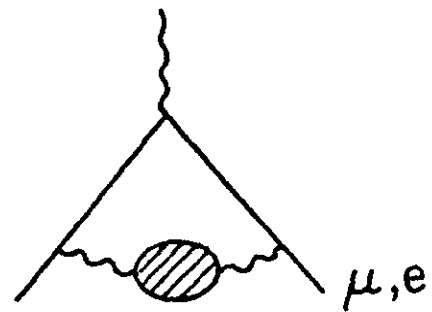


FIG. 2

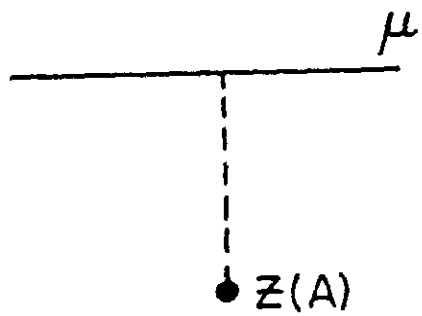




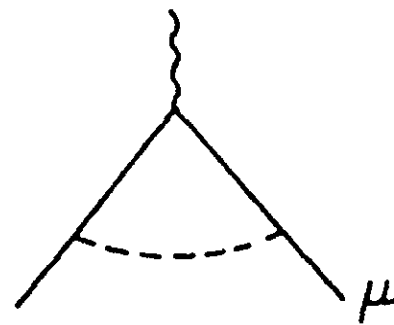
(a)



(b)



(c)



(d)

FIG. 4

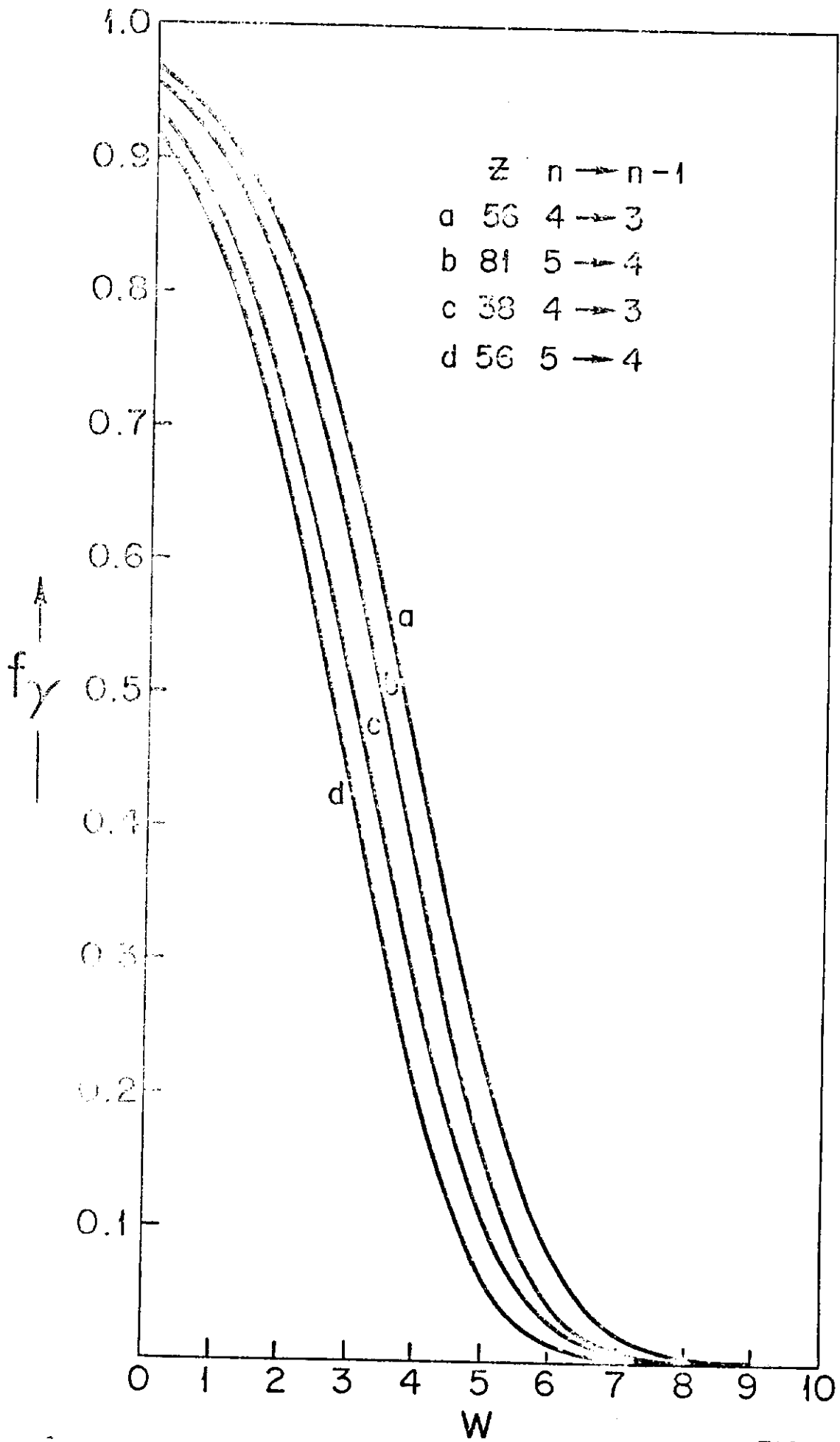


FIG. 5

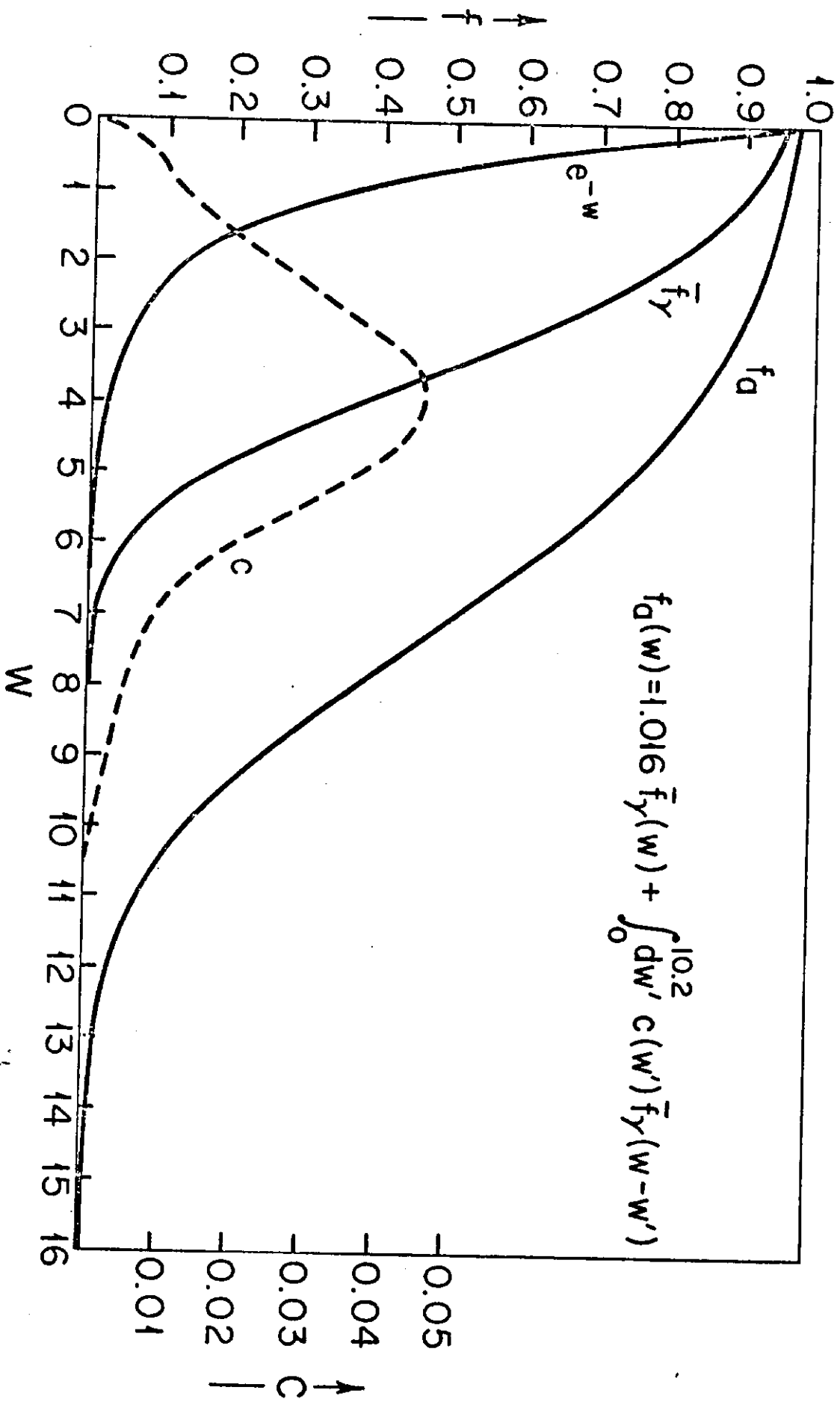


FIG. 6